BSc Thesis Biomedische Technologie

A New Angle on Turn Detection:
A Method for Turn Detection for Varied Angles and Walking Speeds Using IMUs

Noah Sinnema

Supervisor: Michelle van Mierlo PhD Internal
Member: dr. Edwin van Asseldonk External
Member: dr. Jasper Reenalda MSc

July, 2024

Department: Engineering Technology
Faculty: Biomedical Engineering

UNIVERSITY OF TWENTE. | TECHMED CENTRE

Abstract (EN)

In this study, a method was developed for turn detection and turn estimation. This is to distinguish straight from non-straight walking. These turn parameters could provide insight into turn capacity and turn performance to adjust rehabilitation tactics for patients such as the elderly or those suffering from neurological or musculoskeletal diseases such as Parkinson's disease, Alzheimer's disease, multiple sclerosis and osteoarthritis. A turn experiment was done by taking measurements of four healthy individuals with three inertial measurement units (IMU) at slow, preferred and fast walking speeds. The IMUs were placed on the left foot (LF), the right foot (RF) and the sacrum (SA). For filtering a low-pass cutoff frequency of $f_{c,low} = 0.5$Hz was used. Half of the data was the method developed while the other half was used for validation. The mean absolute error (MAE) and the mean relative error (MRE) were used to evaluate the results. The sensor on the SA yielded the best results when estimating turns compared to the LF and the RF. The sensitivity of the turn detection of the combined signal was 100% but with some false positive turns detected. The method is, as a consequence of its design, not able to distinguish turns less than 2s apart from each other. The MAE is the smallest for the SA. Mean values of the MAE for the SA sensor were found to be 3.62°, 3.42°and 3.76°for slow, preferred and fast walking speeds respectively. There was a positive relation between the walking speed and the MAE for the LF and the RF. The lowest and highest MRE values between all Participants, for all angles and the sensor on the SA, were found to be between 1.71% and 8.56%. The MRE is the largest for smaller turn angles. It is recommended to use a 0.5Hz low-pass cutoff frequency when turns are not expected more than once every 2s. Otherwise, a higher low-pass cutoff frequency should be used of up to 1.5Hz. For future research characterising this relation between turn frequency and cutoff frequencies should be examined. Validation with video is yet to be used to find the accuracy of turn duration.

Abstract (NL)

In deze studie is een methode ontwikkeld voor het detecteren en berekenen van bochten. Hiermee kan rechtlijnig van niet-rechtlijnig lopen van elkaar onderscheiden worden. Deze parameters kunnen inzicht bieden in de bocht capaciteit om revalidatiestrategieën aan te passen voor patiëntgroepen als ouderen of mensen die lijden aan neurologische of musculoskeletale aandoeningen zoals de ziekte van Parkinson, de ziekte van Alzheimer, multiple sclerose en osteoartritis. Een experiment werd uitgevoerd door vier gezonde individuen, hierbij werden bochten gemaakt en is dit gemeten met drie inertial measurement units (IMU). Hierbij werd er een langzame, een geprefereerde en een snelle looppas toegepast. De IMU's werden geplaatst op de linkervoet (LF), de rechtervoet (RF) en het sacrum (SA). Voor het filteren werd een laagdoorlaatfilter met een frequentie van $f_{c,low} = 0.5$Hz gebruikt. De helft van de verkregen data werd gebruikt voor de ontwikkelen van de methode. De de andere helft werd gebruikt voor de validatie. De gemiddelde absolute fout (MAE) en de gemiddelde relatieve fout (MRE) werden gebruikt om de resultaten te evalueren. De sensor op het SA leverde de beste resultaten op bij het bereken van de hoek van de bochten in vergelijking met LF en RF. De sensitiviteit van de bochtdetectie van het gecombineerde signaal was 100%, er werd wel één enkele vals-positieve bocht gedetecteerd. De methode is niet in staat om bochten te onderscheiden die minder dan 2 seconden uit elkaar liggen. De MAE is het kleinst voor het SA. Gemiddelde waarden van de MAE voor de SA-sensor waren respectievelijk 3.62°, 3.42°en 3.76°voor de langzame, de geprefereerde en de snelle looppas. Voor de LF en de RF, was een positieve relatie gevonden tussen de loopsnelheid en de MAE. De kleinste en grootste MRE-waarden die tussen alle deelnemers gevonden zijn, voor alle hoeken en voor de sensor op SA, waren tussen 1.71% en 8.56%. De MRE is het grootst voor kleine hoeken. Het is aanbevolen om een laagdoorlaatfrequentie van 0.5Hz te gebruiken wanneer bochten niet vaker dan eens per 2 seconden worden verwacht. Anders moet een hogere laagdoorlaatfrequentie tot 1.5Hz worden gebruikt. Toekomstig onderzoek kan gedaan worden naar de relatie en karakterisatie van de frequentie van bochten en doorlaatfrequenties. Validatie met behulp van video kan worden gebruikt om de nauwkeurigheid van de berekende bocht te bepalen.

Contents

1 Introduction

Free walking mobility is essential for independent living. The risk of falling can diminish quality of life, and independence and can induce fear in high fall risk groups [13]. Control of turning requires a significantly more complex nervous system than straight walking [3]. This is why most falls occur during turning. As victims generally break part of the fall with the femur, there is an eight-times higher chance of breaking the femur during turning compared to straight walking [3]. Many people experience difficulties with mobility such as the elderly or people with movement disorders. Such disorders are neurological or musculoskeletal diseases such as Parkinson's disease (PD), Alzheimer's disease, multiple sclerosis and osteoarthritis [3, 17]. Causes for a change in gait capacity are varied. Some are due to a loss of ability to adjust the walking trajectory in response to surrounding conditions, as some elderly experience [10]. Others, like PD patients with postural instability and gait difficulty (PIDG), suffer from high fall risk due to freezing of gait, postural sway and decreased balance. PIDG patients also performed worse in experiments testing cognitive status and quadriceps muscle strength [13]. Changes in gait capacity can vary greatly between patient groups but can be generalized in changes in cadence, step length, step duration, symmetry in left to right step and turning characteristics [3].

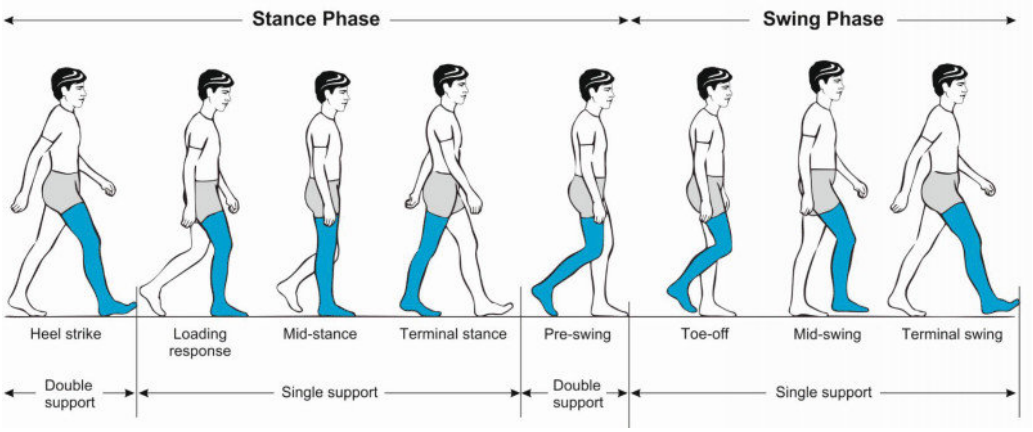

Figure 1: The phases of a gait cycle of a healthy person.

Figure 1 shows the phases of gait of a healthy individual [14]. One gait cycle consists of eight repeating phases. Note that more than half of the gait circle is stationary [14].

Monitoring gait capacity parameters can give valuable insights into how targeted rehabilitation strategies can be applied to achieve better rehabilitation results [3]. Monitoring of gait is most commonly done in a controlled environment using optical motion capture technologies but is limited to this environment [3, 18]. This method is expensive and is also limited to the need for sufficient lighting especially for non-infrared and high-speed cameras [18]. More recent studies also monitored a free-living environment using Inertial Measurement Units (IMU) [3, 7, 9]. This gives a more realistic insight into the overall gait performance of the patient but has its imperfections as a decreased ability of the IMUs to calculate the position reliably. This also presents a new hurdle to discriminate gait from other types of cyclic movements such as cycling and climbing the stairs [7]. Turn monitoring especially can give valuable information for severe injury prevention. Controlled laboratory-based studies of 180°turn detection during gait with PD patients show great sensitivity of 97% [15]. Additionally, other studies focused on the effects of diseases on gait quality, showed the difficulties of monitoring patients with before mentioned diseases [17]. Besides rehabilitation, can monitoring free living help prevent fall-related injuries in high fall-risk groups. Studies have shown that it is possible, while monitoring the gait capacity of the elderly using sensors on the lower limbs in combination with

a statistical model with fall data as input, to discriminate high- from low fall risk patients [3, 5]. In short, monitoring can identify gait capacity and differentiate gait from turns, identify turns during gait, and therefore help with targeted rehabilitation tactics and injury prevention.

In this study, a method is presented to detect turns and estimate absolute turn angles during gait. The aim is to improve on existing methods to consistently detect and estimate turns during gait [3]. This method is designed to distinguish non-straight from straight walking. This can give insight into gait parameters and may be used to alter rehabilitation tactics for the patients. The following research question is asked: Can turn detection be achieved for varied gait velocity and turn angles? It is expected to produce a method with a 90% sensitivity for turn detection [15]. This while aiming for a relative error of 10%. Furthermore, it is expected to see an increase in the absolute error of turn recognition for faster walking speeds [7, 9]. It is furthermore expected that the sensitivity of turn detection will drop when the turn angle reaches 30°angle as it is hard for humans to conduct very slight turns [3]. Lastly, it is expected to see a decrease in the error of the absolute turn estimation of the sensor on the sacrum (SA) compared to the sensor on the left foot (LF) or right foot (RF) [3, 9].

2 Methodology

To develop and later validate the algorithm an experiment was conducted four times. The datasets of two Participants were used to develop the algorithm. the other two datasets were used as validation. With the validation, the sensitivity of turn detection and the error in turn estimation was calculated. The experiments were conducted in a controlled environment. The next sections are the protocol for the experiment and the methodology of the algorithm.

2.1 Experimental Protocol

The experiment was done by taking measurements of four healthy individuals with three IMUs. The IMUs (The Physilog 6S from GaitUp) included triaxial accelerometers, gyroscopes and magnetometers and were recorded at 128 Hz. The IMUs were placed on the LF, the RF and the SA as can be seen in figure 2a and figure 2b [3, 4, 7]. A body-worn GoPro camera was used to film the legs as a verification of the performed experiment [3, 7]. The Participants were instructed to walk on a beforehand determined route with interspersed turns from 30°to 180°. The known route was used as validation of the turn estimation and turn detection. The route resembles half a clock, where the Participants walked from the hour position along the clock hands toward a new hour position. The Participants were instructed to start at position 12, as can be seen in figure 2c, and walk towards the center of the circle with a radius of 10m. At the center, the Participants turned towards position one, two, three, four or five to make a 150°, 120°, 90°, 60°or 30°turn respectively. At the new position, the Participants made a 180°turn and walked back to position 12 via the center of the circle. Each Participant walked the route 30 times, six times per set angle of which two times are at slow speed, two times at preferred speed and two times at fast speed [1, 3]. The IMUs and the camera were restarted after each angle.

(a) Placements of the two IMUs on the left and right foot, attached to the laces of the shoes.

(b) Placement of the third IMU on the sacrum, attached to the belt.

(c) The prescribed route including turns 150°, 120°, 90°, 60°, and 30° turn at positions 1, 2, 3, 4, and 5 respectively.

Figure 2: The placement of the IMUs (figure a and b) and the prescribed route (figure c).

2.2 Algorithm

The following algorithm was developed the programming language Python. The angular velocity (AV), measured by the gyroscope in the xy-plane, is ideal for identifying and measuring turn angles. The IMU measures the AV in its body frame, ω_b. The AV around the body frame is rotated into the inertial reference frame as can be seen in equation 1 [3]

$$\omega_i = q \times \omega_b \times q^{-1}, \tag{1}$$

where $\omega_i \in \mathbb{R}^3$ is the AV in the inertial frame, q is the quaternion, $\omega_b \in \mathbb{R}^3$ is the AV in the body frame and q^{-1} is the inverse of the quaternion. The quaternion is a four-dimensional complex number that follow multiplication rules as can be seen in the quaternion equation 2 [6, 8]

$$i^2 = j^2 = k^2 = ijk = -1, jk = i = -kj, ki = j = -ik, ij = k = -ji, \tag{2}$$

Where i, j and k are complex unit vectors. A more extensive explanation can also be found in the Appendix. The data of the gyroscope can be interpreted as four-dimensional but with one dimension equal to zero. the multiplication of the individual vectors in equation 1 is done performing the Hamilton product as can be seen in the Appendix as equation A1. This is rewritten using the quaternion equation 2 into Appendix equation A2 [6, 8]. Now the z-component of the angular velocity is in the inertial frame and therefore equal to the angular velocity around the vertical axis [3]. This AV is filtered using a low-pass Butterworth filter with a cutoff frequency, $f_{c,low}$, of $f_{c,low} = 0.5$Hz. The $f_{c,low}$ is based on the results of the absolute angle estimation. This filtered AV is later integrated for angle estimation.

The unfiltered AV, $\omega^i_{z,sum}$, of the LF, RF and SA is filtered with a low-pass Butterworth filter with a cutoff frequency of $f_{c,low} = 0.3$Hz and is then summed. The $f_{c,low} = 0.3$Hz is based on the results of the peak selection. Off this new filtered and summed AV peaks are selected over an interval of 2s, to find potential turns, for which the maxima of the AV are -40°/s$\geq \omega^i_{z,sum} \geq$40°/s. The time interval of each turn is determined for which a peak was detected and the thresholds of at least $-5°/s \geq \omega^i_{z,sum} \geq 5°/s$ using the summed AV [3]. The data outside of any turn interval is turned to zero. With these steps, the time interval of each turn is identified. To determine the angle, the filtered AV of LF, RF and SA is separately integrated over time using equation 3.

$$\Theta_z = \int \omega_z = \sum \omega_z dt \tag{3}$$

Where Θ_z is the angle around the z-axis and dt is a discrete-time step [3]. The angle is approximated by summing the multiplication of the AV, ω^i_z, by the time step, dt, as the result of equation 3 presents [3]. Angles are accepted for $\Theta_z \geq 15°$. The trend of the found angles for each walking speed is determined using a linear polyfit function. Lastly, the mean absolute error (MAE) is calculated for the LF, the RF and the SA as can be seen in equation 4 [11].

$$MAE = \frac{1}{n}\sum_{i=1}^{n} |\Theta_{m,i} - \Theta_{t,i}| \tag{4}$$

Where the $\Theta_{m,i}$ is the measured turn angle at the ith position and $\Theta_{t,i}$ is the true turn angle at the ith position. The mean relative error (MRE) is calculated according to equation 5 [16].

$$MRE(\%) = \frac{1}{n}\sum_{i=1}^{n} \frac{|\Theta_{m,i} - \Theta_{t,i}|}{|\Theta_{t,i}|} \cdot 100\% \tag{5}$$

The steps of the method are summarized as a block diagram in figure 3.

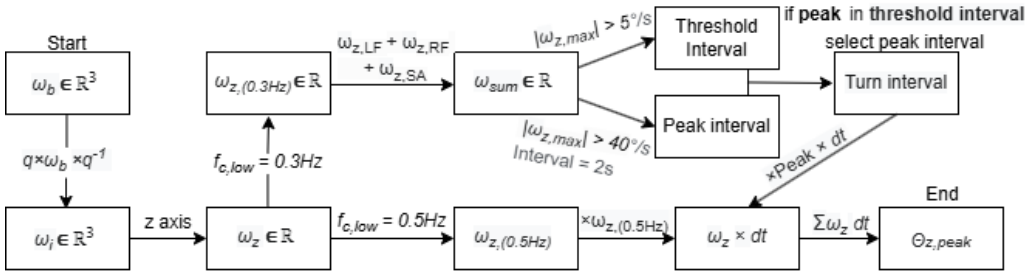

Figure 3: A block diagram summarizing the intermediate steps.

3 Results

Firstly, the experiments were done as prescribed, notes on the experiments can be found in the appendix Table A2, A3, A4 and A5. Secondly, the intermediary results of the algorithm are presented. The results of the unfiltered rotated data compared to rotated filtered data are shown in an AV versus time plot in figures 4, 5, 6 and 7. Each measurement starts with a left-handed turn while each dataset starts with a positive AV peak. Therefore a positive peak in AV and a negative peak in AV can be identified as a left- and right-handed turn, respectively. It can be seen that characteristics of the signal change in that the smoothness increases, the amplitude of the signal decreases and the time duration of the peak increases as $f_{c,low}$ decreases. Thirdly, the AV versus time comparison is shown of three values of $f_{c,low}$ in figure 5, 6 and 7. The two frequencies are the 1.5Hz the literature prescribed and the 0.5Hz 0.3Hz which are chosen after trial and error [1, 3]. Thus the 0.5Hz was chosen after yielding the best angle estimation and the most contrast between peak and non-peak, thus the least error and the least false positive or false negative peak selection, respectively.

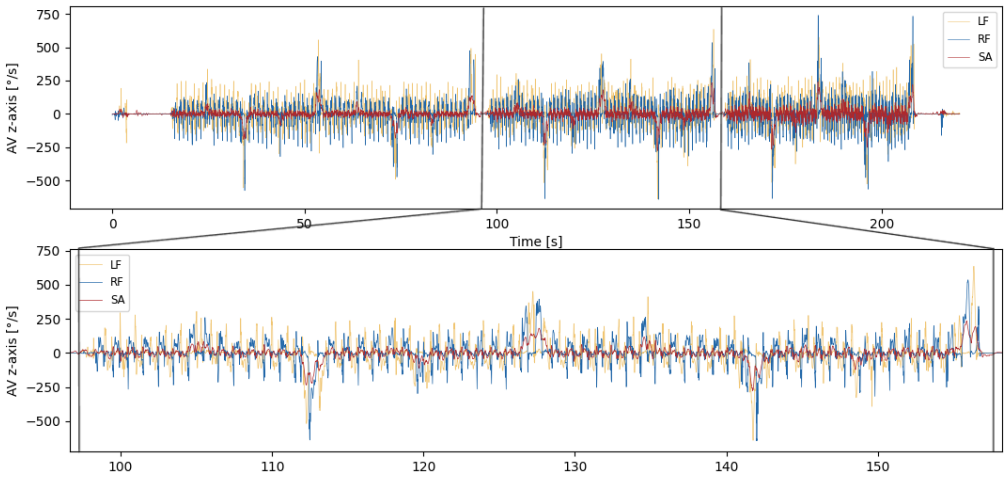

Figure 4: The rotated unfiltered AV vs time of Participant 4 of the prescribed turn of 60°, within the upper graph a representation of the duration of the whole experiment and on the bottom a representation of the preferred speed of the experiment.

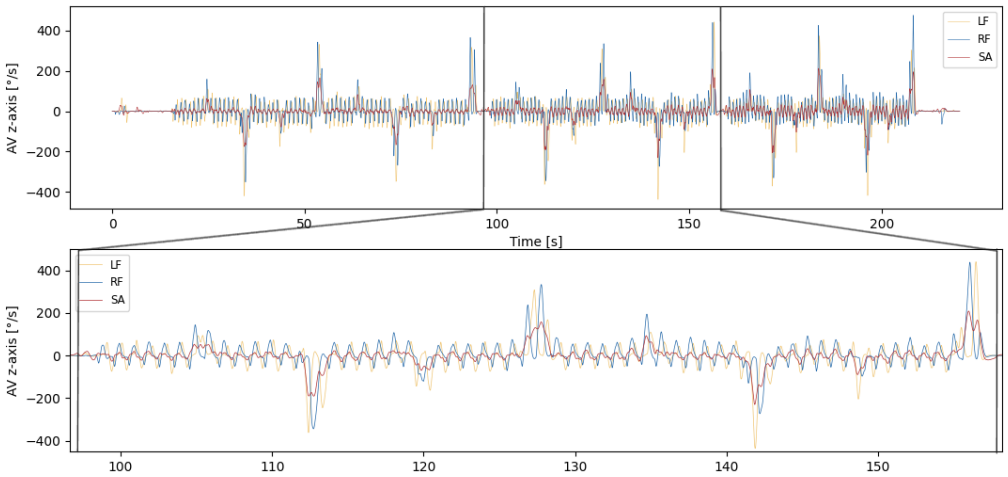

Figure 5: The rotated 1.5Hz low-pass filtered AV vs time of Participant 4 of the prescribed turn of 60°, within the upper graph a representation of the duration of the whole experiment and on the bottom a representation of the preferred speed of the experiment.

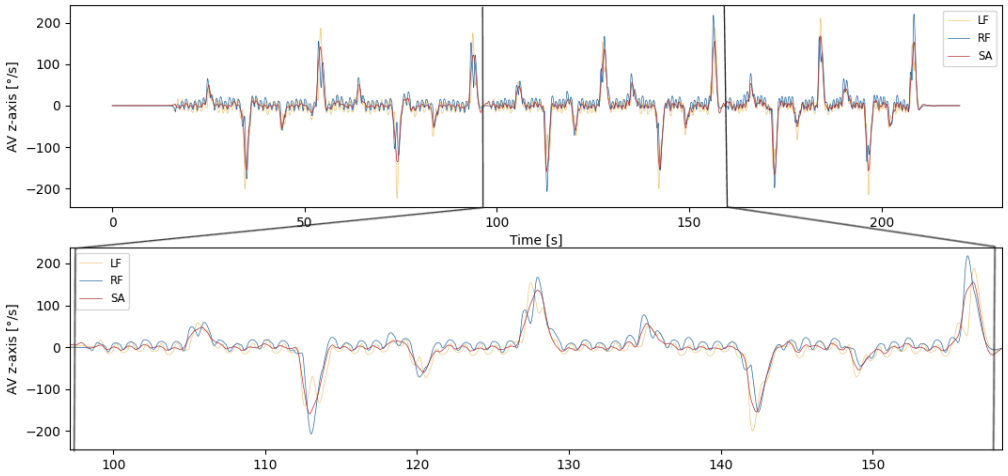

Figure 6: The rotated 0.5Hz low-pass filtered AV vs time of Participant 4 of the prescribed turn of 60°, within the upper graph a representation of the duration of the whole experiment and on the bottom a representation of the preferred speed of the experiment.

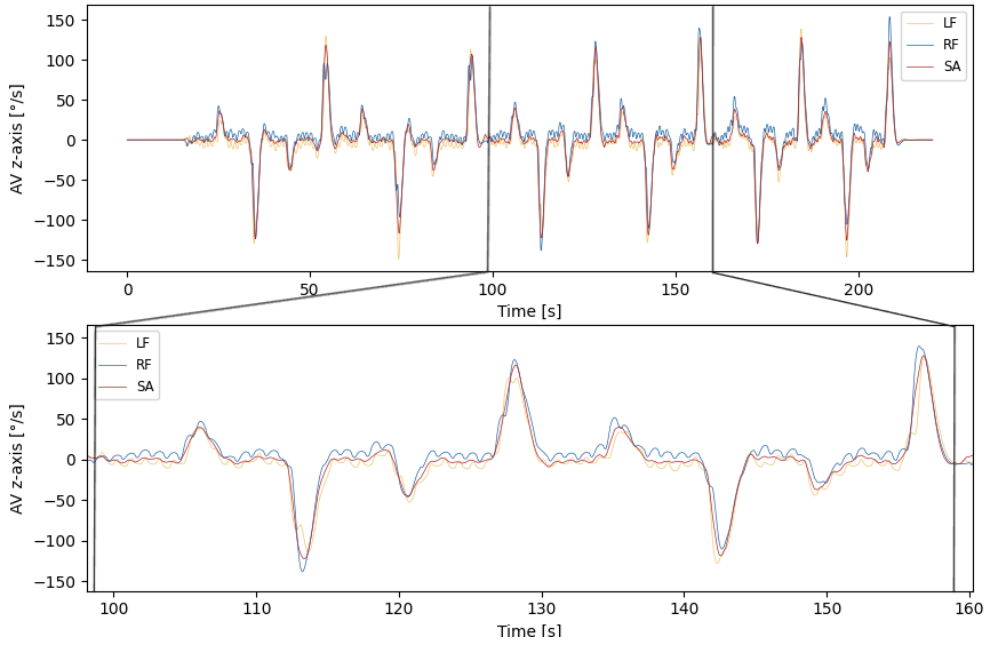

Figure 7: The rotated 0.3Hz low-pass filtered AV vs time of Participant 4 of the prescribed turn of 60°, within the upper graph a representation of the duration of the whole experiment and on the bottom a representation of the preferred speed of the experiment.

The last two figures presenting AV versus time is of the selected peaks. The selected peaks are found by determining the maxima of the summed and low-pass filtered AV at $f_{c,low} = 0.3$Hz as can be seen in the methodology. With this, the interval of each peak is determined. The AV of the LF, RF and SA filtered at $f_{c,low} = 1.5$Hz and $f_{c,low} = 0.5$Hz is presented over the intervals of each turn and can be seen in figure 8 and 9, respectively. It can be seen that the characteristics of the peaks differ, as mentioned before, and that figure 9 presents fewer peaks than figure 8. In both figure 8 and 9 can it be seen that the amplitude of the SA is smaller than those of the LF and RF. Lastly, each measurement starts with a left-handed turn while each dataset starts with a positive AV peak. A positive AV peak and negative AV peak can therefore be identified as a left and right-handed turn, respectively.

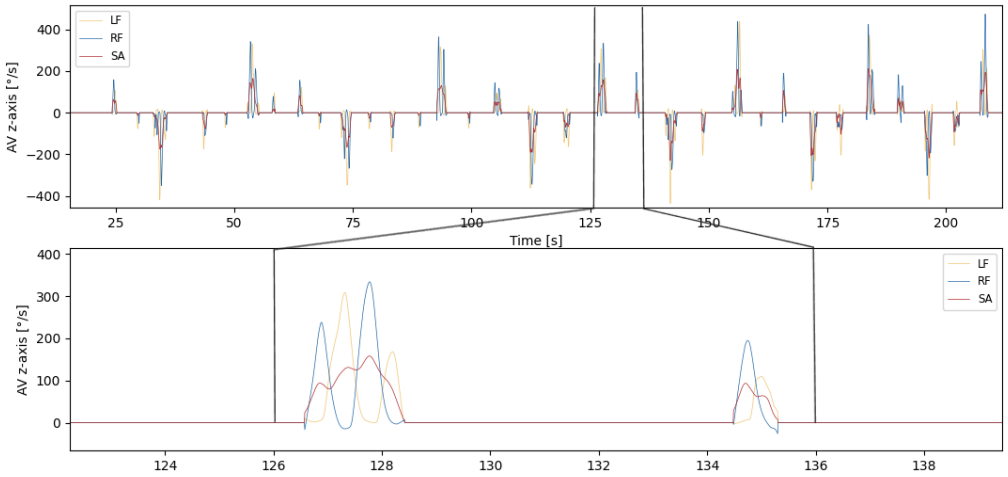

Figure 8: The selected peaks of the 1.5Hz low-pass filtered AV vs time of Participant 4 of the prescribed turn of 60°, within the upper graph a representation of the duration of the whole experiment and on the bottom a representation of one peak during the preferred speed of the experiment.

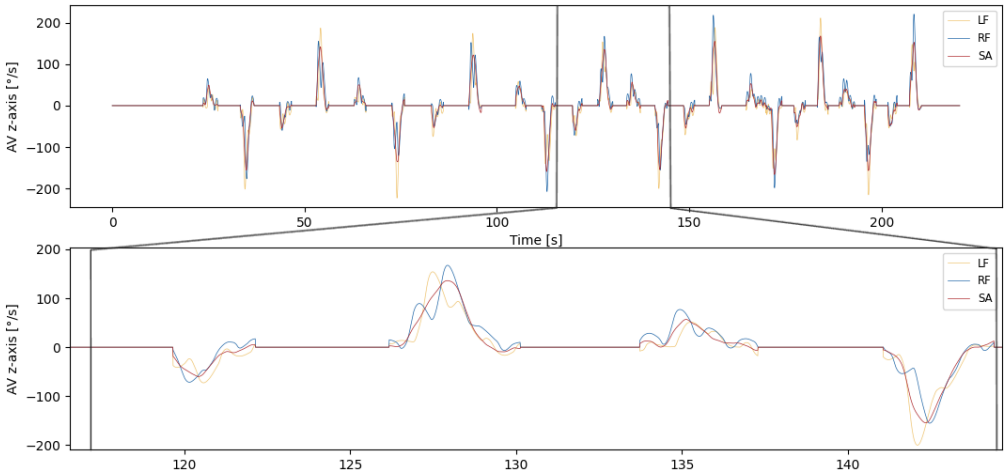

Figure 9: The selected peaks of the 0.5Hz low-pass filtered AV vs time of Participant 4 of the prescribed turn of 60°, within the upper graph a representation of the duration of the whole experiment and on the bottom a representation of one peak during the preferred speed of the experiment.

The next results chronologically present the measured angle [°] versus time [s] of Participants 3 and 4. The LF is denoted by yellow, the RF by blue and the SA by red. The horizontal blue line indicates the value of the prescribed angle and the red line is the measured angles of the SA in time. The red line indicates the oscillating trend of the measurements. It can be seen that the frequency of the red line increases as the walking speed changes from slow, to preferred and to fast. Furthermore, can it be seen that its amplitude is not always equal to the prescribed angle. It can be seen that the LF, RF and SA give varying results, even for the same angle. More specifically can it be seen that the last 180°turn has a trend to fall short of the 180°turn. This can be best seen in figure 10b, 12b, 13a, 13b and especially in 14b. It can also be seen that figure 11b detected an extra turn around the 75s mark. Comparable figures of Participant 1 and 2 can be found in the Appendix figures A1a, A1b, A2a, A2b, A3a, A3b, A4a, A4b, A5a, A5b.

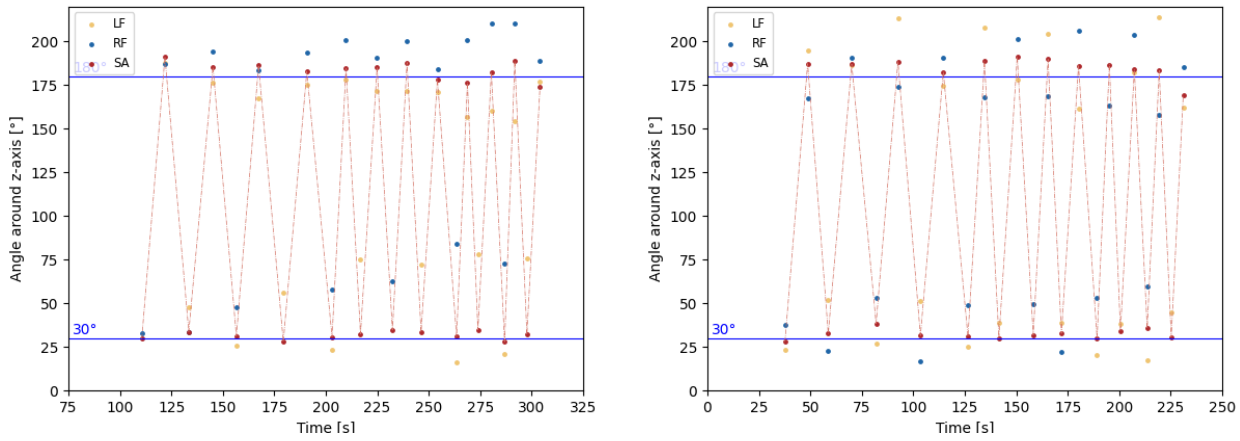

(a) Participant 3. **(b)** Participant 4.

Figure 10: Angle around the z-axis [°] versus time [s] of the prescribed angle of 30°where the LF is denoted by yellow, the RF by blue and the SA by red. The horizontal blue line indicates the value of the prescribed angle and the red line indicates the oscillating trend of the data of the SA in time.

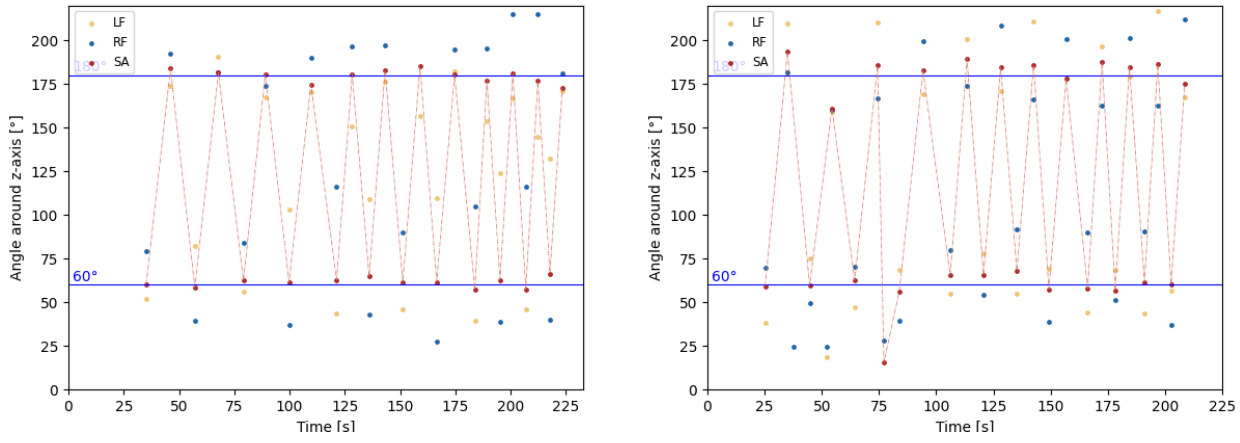

(a) Participant 3. **(b)** Participant 4.

Figure 11: Angle around the z-axis [°] versus time [s] of the prescribed angle of 60°. For a more elaborate explanation 10.

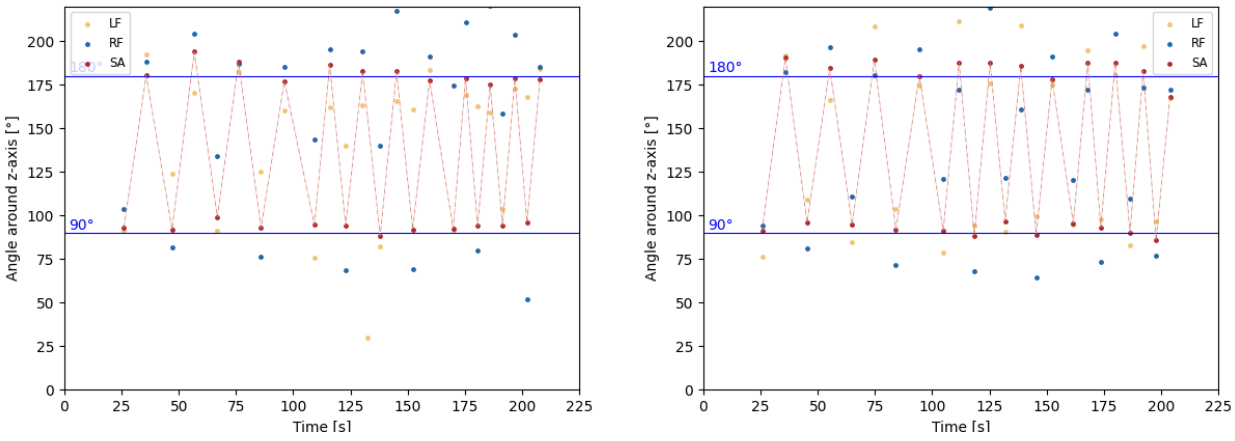

(a) Participant 3. **(b)** Participant 4.

Figure 12: Angle around the z-axis [°] versus time [s] of the prescribed angle of 90°. For a more elaborate explanation 10.

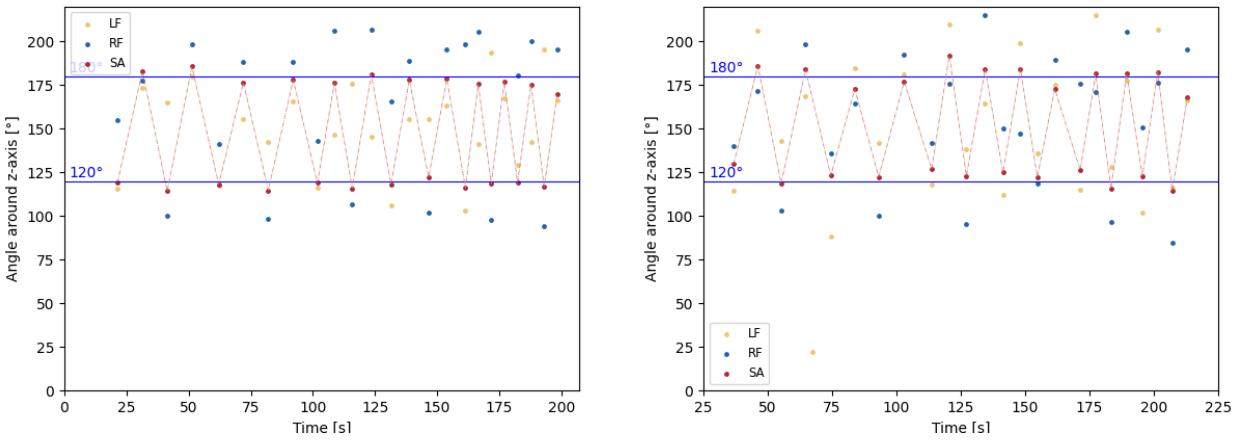

(a) Participant 3. **(b)** Participant 4.

Figure 13: Angle around the z-axis [°] versus time [s] of the prescribed angle of 120°. For a more elaborate explanation 10.

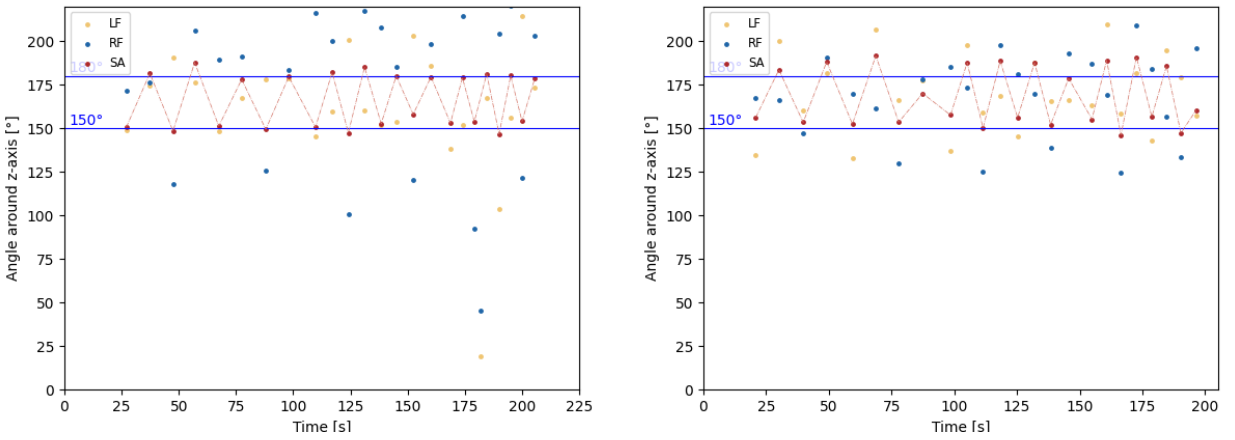

(a) Participant 3. **(b)** Participant 4.

Figure 14: Angle around the z-axis [°] versus time [s] of the prescribed angle of 150°. For a more elaborate explanation 10.

The next figures present the trend the data suggests as can be seen in figure 15 and 16. In this figure the measured angle [°] versus the expected angle [°] of all angles is presented while separating the data of the slow, the preferred and the fast walking speeds of Participants 3 and 4. A linear polyfit trendline of those three subsets is also presented in these figures. It can be seen that all three trendlines are almost identical.

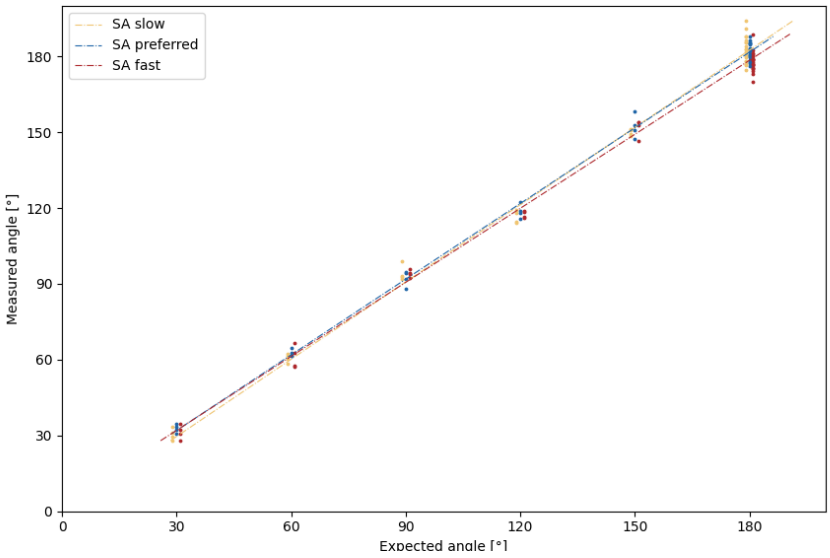

Figure 15: Measured angle [°] versus expected angle [°] of all prescribed angles of Participant 3. Where single data points are presented by dots and the trend is a linear interpolated trendline based on those data points. The slow speed of the SA data is denoted by yellow, the preferred speed of the SA data as blue and the fast speed of the SA data as red.

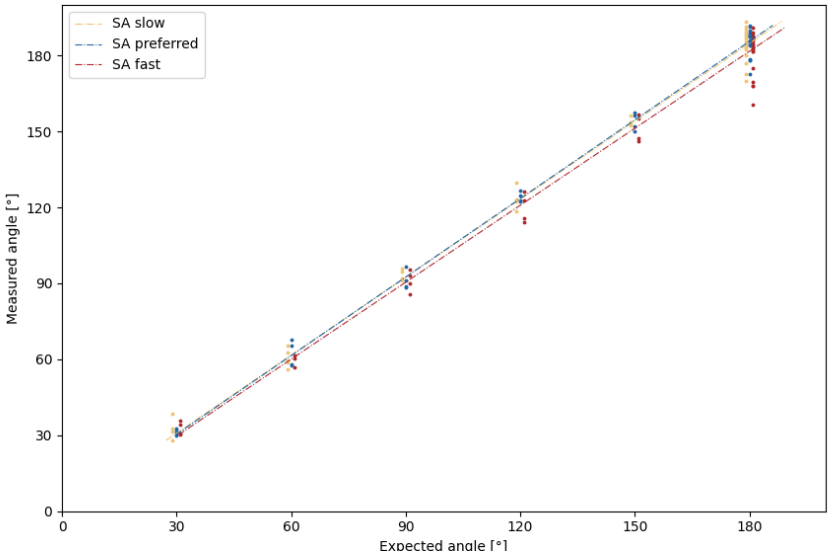

Figure 16: Measured angle [°] versus expected angle [°] of all prescribed angles of Participant 4. Where single data points are presented by dots and the trend is a linear interpolated trendline based on those data points. The slow speed of the SA data is denoted by yellow, the preferred speed of the SA data as blue and the fast speed of the SA data as red.

The final figures, figure 17 and 18, present the absolute error of the data compared to its expected value. In these two figures, the measured angle [°] versus the expected angle [°] is presented while separating the data of the slow, the preferred and the fast walking speeds of Participants 3 and 4. It can be seen that the LF and the RF have an enormous error compared to the SA.

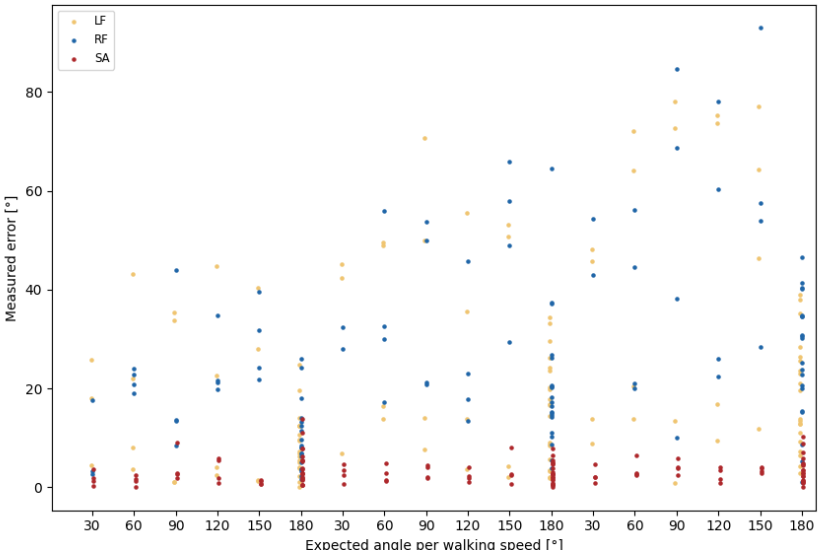

Figure 17: Measured error [°] versus expected angle [°] for all three walking speeds of Participant 3. The LF is represented by yellow, the RF by blue and the SA by red. Each walking speed is presented in its interval of 30°to 180°with on the left the slow speed, in the middle the preferred speed and on the right the fast speed of the LF, RF and SA.

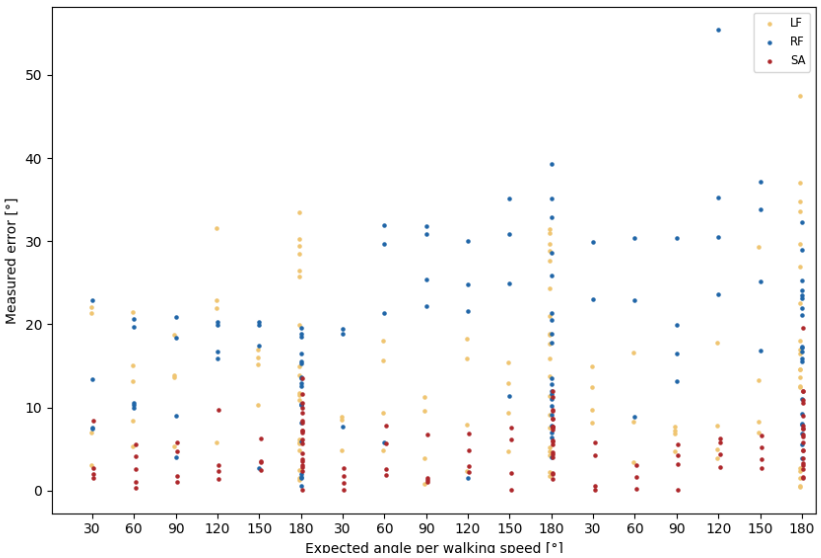

Figure 18: Measured error [°] versus expected angle [°] for all three walking speeds of Participant 4. The LF is represented by yellow, the RF by blue and the SA by red. Each walking speed is presented in its interval of 30°to 180°with on the left the slow speed, in the middle the preferred speed and on the right the fast speed of the LF, RF and SA.

The MAE of each angle is presented by all Participants for the sensor on the LF, RF and SA for slow, preferred and fast walking speeds as can be seen in Table 1. The MAE of Participants 1 to 4 for the sensor on the LF, RF and SA for slow, preferred and fast walking speeds. It can be seen that the MAE is the smallest for the SA. Furthermore, can it be seen that the MAE is the smallest for slow walking speeds, where especially the LF and the RF are very sensitive to a change in walking speed.

Table 1. The MAE [°] of Participants 1 to 4.

	Slow LF [°]	Preferred LF [°]	Fast LF [°]	Slow RF [°]	Preferred RF [°]	Fast RF [°]	Slow SA [°]	Preferred SA [°]	Fast SA [°]
Participant 1	10.12°	16.45°	16.49°	8.43°	15.99°	14.66°	2.45°	2.69°	2.87°
Participant 2	12.80°	16.13°	15.55°	5.57°	7.39°	7.28°	3.68°	3.07°	3.49°
Participant 3	13.41°	23.20°	30.05°	15.35°	27.58°	36.40°	3.38°	2.92°	3.38°
Participant 4	14.83°	13.01°	14.13°	12.88°	19.76°	21.30°	4.96°	5.00°	5.31°
Mean	12,79°	17,20°	19,06°	10,56°	17,68°	17,35°	3,62°	3,42°	3,76°

The MRE is presented in Table 2. Here the MRE [%] angle of each turn is separately calculated and presented. The MRE of Participants 1 to 4 for all angles for the sensor on the LF, RF and SA. It can be seen that the MRE is the smallest for the SA. Furthermore, can it be seen that the MRE tends to get smaller when the turn angles get larger.

Table 2. The MRE [%] of Participants 1 to 4.

	30°	60°	90°	120°	150°	180°
LF of Participant 1	26.30%	34.90%	20.51%	16.89%	17.64%	5.50%
RF of Participant 1	35.01%	26.11%	22.80%	12.07%	13.83%	5.37%
SA of Participant 1	4.16%	3.15%	2.40%	2.27%	2.17%	1.71%
LF of Participant 2	46.64%	29.50%	20.22%	12.18%	8.68%	7.86%
RF of Participant 2	19.03%	17.34%	11.20%	5.55%	4.19%	3.15%
SA of Participant 2	6.18%	2.46%	2.68%	2.09%	1.75%	2.58%
LF of Participant 3	85.33%	52.27%	35.13%	24.85%	21.19%	8.10%
RF of Participant 3	96.37%	50.58%	39.54%	26.72%	30.70%	10.37%
SA of Participant 3	7.81%	4.25%	4.22%	2.30%	1.78%	2.02%
LF of Participant 4	35.62%	18.94%	9.59%	11.19%	8.81%	9.10%
RF of Participant 4	60.73%	31.74%	22.42%	20.51%	15.30%	8.33%
SA of Participant 4	8.56%	4.88%	3.41%	3.65%	2.77%	3.76%

4 Discussion

The goal of this paper is to develop a method for detecting turns and estimating the turn angle. This is to distinguish straight from non-straight walking. These turn parameters could provide insight into how to adjust rehabilitation tactics for patients suffering from neurological or musculoskeletal diseases. The MAE is the smallest for the SA as can be seen in Table 1. This is in accordance with Micó-Amigo et al. and El-Gahory et al. [3, 9]. The mean values of the MAE for the SA sensor were found to be 3.62°, 3.42°and 3.76°for slow, preferred and fast walking speeds respectively. An increase in MAE was only found for the LF and RF for increasing walking speeds as can be seen in Table 2. This was expected for all sensors. This is thus partly in line with what was expected from Micó-Amigo et al. and Hickey et al. [7, 9]. The MRE was for all Participants and all angles under 10%. MRE values, chosen from all Participants and angles for the sensor on the SA, were found to be between 1.71% and 8.56%. The MRE is the largest for smaller turn angles. The MRE was smaller than expected for the SA but much larger for the LF and RF. Furthermore, a low-pass cutoff frequency of $f_{c,low}$ = 0.5Hz has great turn detection and turn estimation ability. The sensitivity of the turn detection of the combined signal was 100%, which was higher than expected. The expectation was based on Rehman et al. [15]. Turn sensitivity did not significantly drop when reaching turn angles of 30°, as was previously expected and described by El-Gahory et al. [3]. A false positive measurement did occur.

The data of Participant 1 and 2 was specifically collected for the development of the algorithm. This data was used to make the algorithm and thus was designed to minimize the error. The results of these Participants are therefore left in the Appendix. The reader is advised to place the results of Participant 1 and 2 into this context. It was expected to find substantial difference in the error estimation between the two types of datasets, as was the case. Furthermore, contrary to the original methodology, was the algorithm altered after reviewing the first results of Participant 4. Namely thresholds and cutoff frequencies were altered. In the end are all results made with the same algorithm with the same thresholds and cutoff frequencies.

4.1 Experimental Uncertainties

The experimental setup, made by hand using measurement tape and chalk, was sensitive to incidental errors in the proportions. This may have caused an error of up to 5°in the setup compared to the expected value. Therefore should another form of validation be used in the future such as optical motion capture [3, 18]. Furthermore, the setup of the experiment was made two times, first for Participants 1 and 2 and second for Participants 3 and 4. This introduces different incidental errors in the known angle for those two Participant groups. Calculating the standard deviation may give better insight into the behavior of the data as this is not dependable on any known angles. The second difficulty regarding angles has to do with the turn behavior of the subjects. Subjects might turn in different ways and make adjustments during the straight walking. The algorithm is not sensitive enough to detect small corrections. So besides the error in the turn setup of the experiment, this might also introduce a small in the error estimation. It is hard to define a turn in the first place. Some solutions may be using discrete intervals, velocity vectors, or positions over time. All fall short of a perfect description of the turn behavior of the subject. In this paper, discrete intervals are used to define turns.

To ensure thoroughness, both left- and right-handed turns were performed. But the method does not specify if, at the 180°turn, a left- or right-handed turn should be taken. When comparing the data of Participants one, two, three and four it is evident whether the subjects have a preferred turn direction. It is, however, not the case that this leads to worse results. Moreover, the last angle typically shows the largest error. This can partly be due to the experimental setup. This last turn, always

a turn of 180°, was the last task of the experiment. No straight walking took place after this turn. Participants, instead of immediately walking, stayed stationary after this last turn. This stationary turn may have influenced the turn that the Participants made, as no destination was fixed for them to walk toward. there may have been an error introduced due to a partly executed turn.

4.2 Remarks on the Results

In the enlarged bottom part of figure 8 two sets of peaks can be seen. The first set of peaks is collectively the AV of a 180°and the second of a 60°turn, both in positive (left) direction. It can be seen that the AV for the LF and RF 180°turn has two separate peaks. The AV signal is split into multiple peaks. This happens when the feet are at a stationary part of the gait cycle and thus a phenomenon solely of the feet. The LF and RF are always half a phase out of phase as always one foot needs to be on the ground. This phenomenon makes it difficult to find the maximum peak of those individual signals. Furthermore, the signal can alternate between positive and negative values, which makes it seem like multiple turns are made instead of one big turn. To avoid this a combination of at least two sensors is needed. This can be either the sensor on the sacrum combined with one on the foot or only both feet. In this method, this summing of signals is important to detect the AV peak values of a turn. This is contrary to previous research of El-Gohory et al. [3]. In El-Gohory et al. only positive or negative peaks are detected, separately [3]. The method of this paper is different, where it argues that a turn of a single sensor can be composed of multiple smaller AV peaks, as long as the summed AV signal of multiple sensors is the same sign during the whole turn. Thus the route of the AV signal does not matter like a function of state.

It seems like Participant 4 suffers from the largest error, as the final calculation for the mean error would suggest. This can be partly explained by the large error at around 55s and the false positive measurement around 75s, which can be both seen in figure 11b. The algorithm did not perform significantly worse compared to Participant 3. This is why it seems the walking behavior of Participant 4 did not influence the calculation of the absolute turn more than other Participants.

4.3 Limitations of the Algorithm

It was expected to get adequate results when applying a low-pass filter with a cutoff frequency of 1.5Hz as the literature about gait analysis presented [1, 3]. But it was found that best results were found at a much lower frequency of 0.5Hz. For finding the maxima of the AV of the combined LF, RF, SA signal a 0.3Hz low-pass filter was used for best results. Gait frequency is still recognisable with a cutoff low-pass frequency of 1.5Hz [2]. For this method of turn detection is this not valuable information, and can lower cutoff frequencies be used. Filtering with a low cutoff frequency such as $f_{c,low} = 0.5$Hz make the signal much longer in time and the amplitude much smaller compared to the unfiltered signal. This method still yields good results, implying the total surface area under the AV curve stays constant. So while the amplitude greatly decreased did the signal lengthen, resulting in a comparable quality the results. This means that the duration of the turn, artificially, increased from approximately 2s to 4s for the 180°turn when comparing the 1.5Hz to the 0.5Hz cutoff frequency as can be seen in figures 8 and 9. However, this algorithm is beneficial for the contrast of the peaks versus the surrounding signal. This can be leveraged to detect turns but does have the drawback of a declined peak amplitude when the cutoff frequency reaches 0.5Hz. Thus a decrease of the cutoff frequency also decreases the maximum sample frequency of the algorithm to detect turns while increasing the contrast of the peaks versus the surrounding signal.

It was found that drift did not occur. Therefore an high past filter or a de-drift function was not applied. This is contrary to papers such as of Greene et al. using a high-pass filter and Nguyen et al.

using a detrend function [5, 12]. Both a high pass Butterworth filter with a cutoff frequency of $f_{c,high}$ = 0.0025Hz and a detrend function were tried but not beneficial for turn estimation [5]. Integration of the AV can effect the MAE when drift is present. Integration over time systematically sums up the product of the AV and the *dt* and thus the sum of the error. Integration over time is thus sensitive to low frequency drift of the signal. Slow turns of a longer duration are therefore more affected by drift than fast turns of short duration.

Furthermore, can it be seen in the top of figure 8 that the peak selection function over selects peak and is thus too sensitive. This is due to the need for a low threshold for the 30°turn. Additionally the function for selecting peaks is limited by two parameters: cutoff peak amplitude and peak interval. The lowest AV threshold of a 30°turn was slightly higher than the selected cutoff value of 40°/s. While the interval over which the peak was the maximum value was selected to be 2s. So the peak is the maximum value for an interval of at least the coming 1s and the past 1s. But this still leaves an overestimation of peaks. Some of the false positive angles will be discarded as integration of the false positive peaks, which tend to have low AV values, lead to small angles. Some of the angles are smaller than $\Theta < 15°$and can be eliminated. The time frame of the peak detection is 2s, this is done as this is consistent with the time frame of the 0.5Hz cutoff frequency low-pass filter, which can identify frequencies with a phase of 2 seconds. At last, a turn is defined as an AV higher than 5 degrees per second. This makes the absolute turn estimation a little less as part of the AV signal is deleted. This error is slightly higher due to the flattening of the peak amplitude as discussed previously.

4.4 future research

The focus of this paper is limited to turns. Other gait capacity parameters are not measured. Walking speed is recognized as an important parameter in turn detection and turn estimation [1, 3]. However, the frequency of turns has not yet been extensively tested. For future research, it may be useful to characterize the limitations of the algorithm for increased turn frequencies in combination with varied walking speeds. This can be done by conducting the same experiment as proposed in the method but with a circle radius of less than 10 meters. Another way to test the algorithm would be by conducting a free-living experiment to determine if the algorithm holds for less predictable gait behavior.

Also, for future research might a combination of high-performance methods be useful to be able to characterize the gait capacity and turn capacity of the patient more completely. Recent papers already attempt to do so like El-Gahory et al. Martin et al. and Hickey et al. [3, 7, 17]. Other studies found distinguishing high fall risk groups from low fall risk groups is possible [3, 5]. The method as proposed by Greene et al. was to monitor gait capacity and gait performance in combination with fall data of the same patient group [5]. This was used to make a statistical model that associates gait performance with fall risk. A similar model can be designed that associates turn capacity and turn performance with fall data. This is to discriminate high fall-risk groups from low by monitoring these gait parameters. This can be employed to implement preemptive measures. There is still demand for fall prevention. Studies have shown, that for PD patients and the elderly, some 45% to 68% of people with PD fall each year, with steadily rising risk of fracture after 40 years of life [13]. This makes the fall risk of PD patients a staggering four times higher than non-PD peers [13]. While of the elderly living in a long-term setting 30% to 50% fall each year, of which 40% fall more than once [5]. Making it the most common cause of injury and hospitalization for the elderly [5].

5 Conclusion

In this study a method is developed for turn detection and turn estimation. The sensor on the SA yields the best results when estimating turns compared to the LF and the RF. At least two sensors should be used for turn detection. The 1.5Hz low-pass cutoff frequency is oversensitive to in turn detection. The 0.5Hz low-pass cutoff frequency provides best results and is able to detect all turns. It is not able to distinguish turns that are less than 2s apart from each other. There is a positive relation between the walking speed and the error for the LF and the RF. There is little relation between walking speed and the error for the SA. It is recommended to use the 1.5Hz low-pass cutoff frequency for when turns occur more than once every 2s. Otherwise the 0.5Hz low-pass cutoff frequency should be used for best results.

This paper shows that turn detection and turn estimation is possible for varied circumstances. Such key gait parameters can therefore be monitored on rehabilitating patients and provide insight in their turn capacity and turn performance. Ultimately could this method be used to distinguish straight walking from non-straight walking in an effort to better the rehabilitation tactics used on patients with neurological or musculoskeletal diseases.

References

[1] Matilde Bertoli, Andrea Cereatti, Diana Trojaniello, Andrea Ravaschio, and Ugo Della Croce. The identification of multiple u-turns in gait: comparison of four trunk imu-based methods. 12 2016.

[2] Philip Crowell, Angela Boynton, and Michael Mungiole. Exoskeleton power and torque requirements based on human biomechanics. 2002.

[3] Mahmoud El-Gohary, Sean Pearson, James McNames, et al. Continuous monitoring of turning in patients with movement disability. *Sensors (Basel)*, 14(1):356–369, 2013.

[4] Gait Up SA. *Physilog 6S User Manual*. Gait Up SA, EPFL Innovation Park, Batiment C, CH-1015 Lausanne, Switzerland, v1.0.0 edition, January 2021. Date: 08.01.2021.

[5] B. R. Greene, E. P. Doheny, C. Walsh, C. Cunningham, L. Crosby, and R. A. Kenny. Evaluation of falls risk in community-dwelling older adults using body-worn sensors. *Gerontology*, 58(5):472–480, 2012.

[6] William Rowan Hamilton. On quaternions, or on a new system of imaginaries in algebra. *Philosophical Magazine and Journal of Science*, 1844-1850. Edited and with a note on the text by David R. Wilkins, March 2000.

[7] Aodhán Hickey, Silvia Del Din, Lynn Rochester, and Alan Godfrey. Detecting free-living steps and walking bouts: validating an algorithm for macro gait analysis. *Physiol Meas*, 38(1):N1–N15, 2017.

[8] Yan-Bin Jia. Quaternions and rotations, September 10 2013. Com S 477/577 Notes.

[9] M Micó-Amigo, T Bonci, A Paraschiv-Ionescu, et al. Assessing real-world gait with digital technology? validation, insights and recommendations from the mobilise-d consortium. *Journal of NeuroEngineering and Rehabilitation*, 20(1):78, 2023.

[10] T. Nakamura, K. Kodama, J. Sakazaki, and T. Higuchi. Relationship between adaptability during turning and the complexity of walking before turning in older adults. *Journal of Motor Behavior*, 55(4):331–340, 2023.

[11] Tereza Nečasová, Ninon Burgos, and David Svoboda. Chapter 25 - validation and evaluation metrics for medical and biomedical image synthesis. In Ninon Burgos and David Svoboda, editors, *Biomedical Image Synthesis and Simulation*, The MICCAI Society book Series, pages 573–600. Academic Press, 2022.

[12] H.P. Nguyen, F. Ayachi, C. Lavigne–Pelletier, et al. Auto detection and segmentation of physical activities during a timed-up-and-go (tug) task in healthy older adults using multiple inertial sensors. *Journal of NeuroEngineering and Rehabilitation*, 12(1):36, 2015.

[13] P. H. S. Pelicioni, J. C. Menant, M. D. Latt, and S. R. Lord. Falls in parkinson's disease subtypes: Risk factors, locations and circumstances. *International Journal of Environmental Research and Public Health*, 16(12):2216, 2019.

[14] Walter Pirker and Regina Katzenschlager. Gait disorders in adults and the elderly: A clinical guide. *Wiener klinische Wochenschrift*, 129, 10 2016.

[15] Rana Zia Ur Rehman, Philipp Klocke, Sofia Hryniv, Brook Galna, Lynn Rochester, Silvia Del Din, and Lisa Alcock. Turning detection during gait: Algorithm validation and influence of sensor location and turning characteristics in the classification of parkinson's disease. *Sensors (Basel, Switzerland)*, 2020.

[16] Chris Tofallis. Measuring relative accuracy: A better alternative to mean absolute percentage error. *SSRN Electronic Journal*, 01 2013.

[17] Martin Ullrich, Arne Küderle, Julius Hannink, Silvia Del Din, Heiko Gaßner, Franz Marxreiter, Jochen Klucken, Bjoern M. Eskofier, and Felix Kluge. Detection of gait from continuous inertial sensor data using harmonic frequencies. *IEEE Journal of Biomedical and Health Informatics*, 24(7):1869–1878, 2020.

[18] L. Wade, L. Needham, P. McGuigan, and J. Bilzon. Applications and limitations of current markerless motion capture methods for clinical gait biomechanics. *PeerJ*, 10:e12995, 2022.

Appendices

.1 The Hamilton Product

W. R. Hamilton is credited with having developed quaternions in 1843 while walking along the Broom Bridge. It was there that he had the idea of the quaternion and to his delight engraved the famous quaternion equations into the bridge [8]. The quaternion is a four-dimensional complex number system to describe the rotation in three dimensions. Quaternions are formulated as $q = a+b\mathbf{i}+c\mathbf{j}+d\mathbf{k}$, where $\mathbb{H} = \{a + b\mathbf{i} + c\mathbf{j} + d\mathbf{k} : a, b, c, d \in \mathbb{R}^3\}$, a hypercomplex number which follow the rules of the quaternion equations of equation 2 [6, 8]. The rotation of a point can be done by multiplying it with its quaternion and its inverse, like equation 1. Where the inverse of a quaternion is obtained by changing the sign of its imaginary parts. Each multiplication of two quaternions is calculated using the Hamilton product [6, 8]. The Hamilton product of two elements:
$q_1 = a_1 + b_1\mathbf{i} + c_1\mathbf{j} + d_1\mathbf{k}$ and $q_2 = a_2 + b_2\mathbf{i} + c_2\mathbf{j} + d_2\mathbf{k}$

$$
\begin{aligned}
q_1q_2 &= (a_1 + b_1\mathbf{i} + c_1\mathbf{j} + d_1\mathbf{k})(a_2 + b_2\mathbf{i} + c_2\mathbf{j} + d_2\mathbf{k}) \\
&= a_1a_2 + a_1b_2\mathbf{i} + a_1c_2\mathbf{j} + a_1d_2\mathbf{k} \\
&+ b_1a_2\mathbf{i} + b_1b_2\mathbf{i}^2 + b_1c_2\mathbf{ij} + b_1d_2\mathbf{ik} \\
&+ c_1a_2\mathbf{j} + c_1b_2\mathbf{ji} + c_1c_2\mathbf{j}^2 + c_1d_2\mathbf{jk} \\
&+ d_1a_2\mathbf{k} + d_1b_2\mathbf{ki} + d_1c_2\mathbf{kj} + d_1d_2\mathbf{k}^2 \qquad \text{(A1)} \\
&= a_1a_2 - b_1b_2 - c_1c_2 - d_1d_2 \\
&+ (a_1b_2 + b_1a_2 + c_1d_2 - d_1c_2)\mathbf{i} \\
&+ (a_1c_2 - b_1d_2 + c_1a_2 + d_1b_2)\mathbf{j} \\
&+ (a_1d_2 + b_1c_2 - c_1b_2 + d_1a_2)\mathbf{k} \qquad \text{(A2)}
\end{aligned}
$$

Table A1. The timeframe for which the data was set to zero outside the time interval of the experiment from the front and back [s].

	30°	60°	90°	120°	150°
Participant 1	100s, 6s	22s, 5s	13s 9s	13s, 13s	16s, 10s
Participant 2	26s, 7s	18s, 10s	21s 11s	23s, 5s	22s, 8s
Participant 3	95s, 22s	22s, 7s	14s, 7s	9s, 7s	14s, 7s
Participant 4	24s, 12s	14s, 7s	13s, 15s	25s, 11s	8s, 7s

.2 Remarks During the Experiments

The interruptions did not occur during any turns and did not interfere with the data collection.

Table A2. Disturbances encountered for every measurement taken as prescribed in the experiment protocol of Participant 1. ” can be read as 'No comment'.

Measurement, angle	Slow	Preferred	Fast
1, 30°	”	”	”
2, 60°	”	”	”
3, 90°	”	”	”
4, 120°	”	”	”
5, 150°	”	”	”

Table A3. Disturbances encountered for every measurement taken as prescribed in the experiment protocol of Participant 2. ” can be read as 'No comment'.

Measurement, angle	Slow	Preferred	Fast
1, 30°	”	”	”
2, 60°	”	”	”
3, 90°	”	”	Interruption by biker
4, 120°	”	”	Interruption by biker
5, 150°	”	”	”

Table A4. Disturbances encountered for every measurement taken as prescribed in the experiment protocol of Participant 3. ” can be read as 'No comment'.

Measurement, angle	Slow	Preferred	Fast
1, 30°	”	”	Sensor of RF moved
2, 60°	”	”	”
3, 90°	”	”	”
4, 120°	”	”	”
5, 150°	”	”	”

Table A5. Disturbances encountered for every measurement taken as prescribed in the experiment protocol of Participant 1. ” can be read as 'No comment'.

Measurement, angle	Slow	Preferred	Fast
1, 30°	”	”	”
2, 60°	”	”	”
3, 90°	”	”	”
4, 120°	”	”	”
5, 150°	”	”	”

.3 Results of Participants 1 and 2

The next results chronologically present the measured angle [°] versus time [s] of Participants 1 and 2. The LF is denoted by yellow, the RF by blue and the SA by red. The horizontal blue line indicates the value of the prescribed angle and the red line is the measured angles of the SA in time. The red line indicates the oscillating trend of the measurements. It can be seen that the frequency of the red line increases as the walking speed changes from slow, to preferred and to fast. Furthermore, can it be seen that its amplitude is not always equal to the prescribed angle.

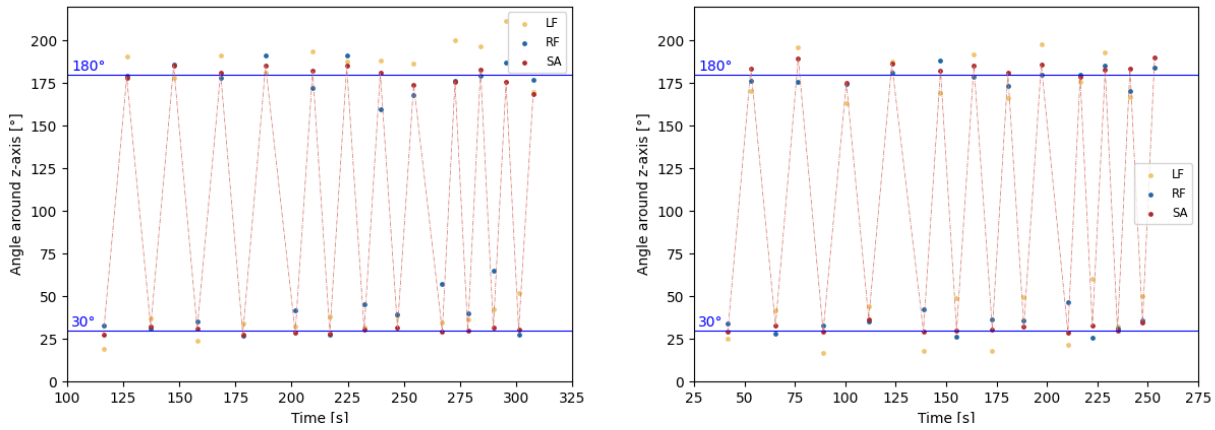

(a) Participant 1. **(b)** Participant 2.

Figure A1: Angle around the z-axis [°] versus time [s] of the prescribed angle of 30°where the LF is denoted by yellow, the RF by blue and the SA by red. The horizontal blue line indicates the value of the prescribed angle and the red line indicates the oscillating trend of the data of the SA in time.

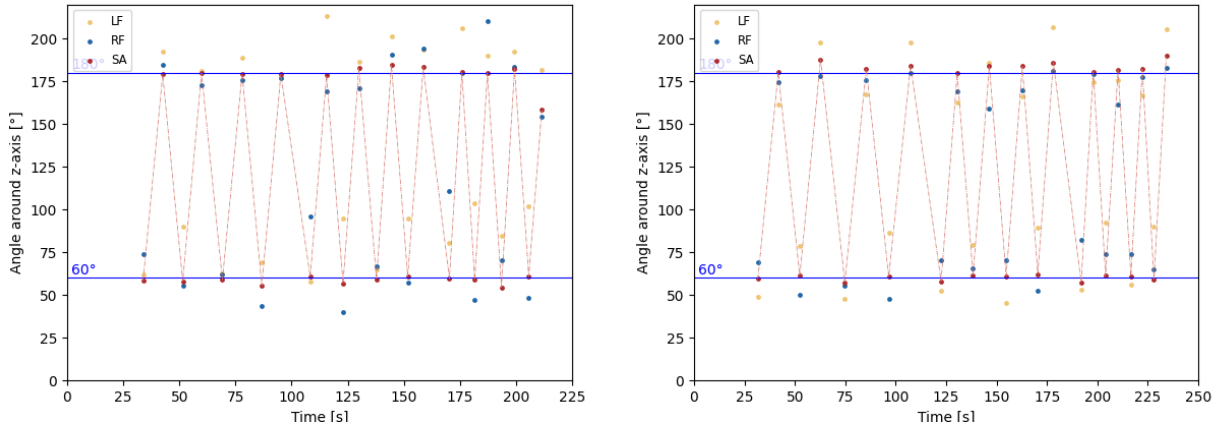

(a) Participant 1. **(b)** Participant 2.

Figure A2: Angle around the z-axis [°] versus time [s] of the prescribed angle of 60°. For a more elaborate explanation 10.

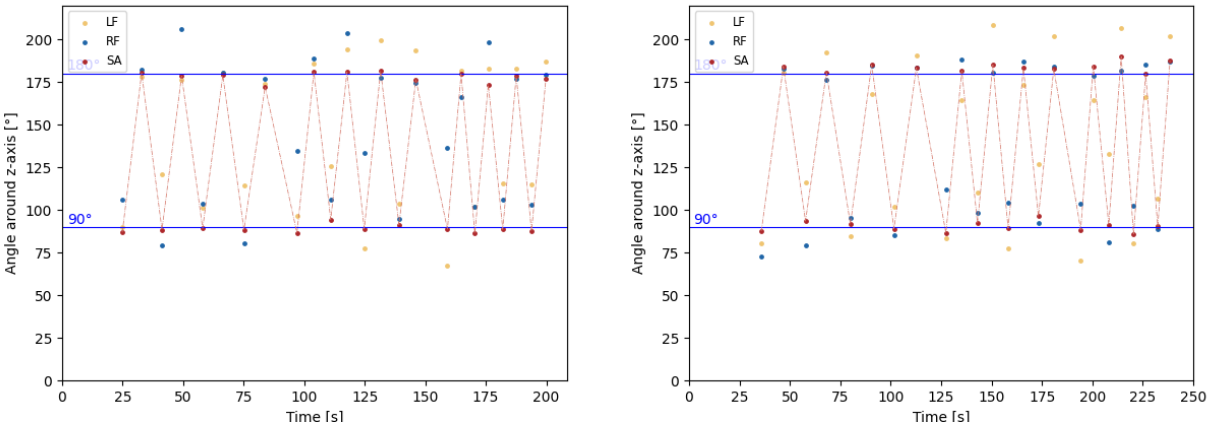

(a) Participant 1. **(b)** Participant 2.

Figure A3: Angle around the z-axis [°] versus time [s] of the prescribed angle of 90°. For a more elaborate explanation 10.

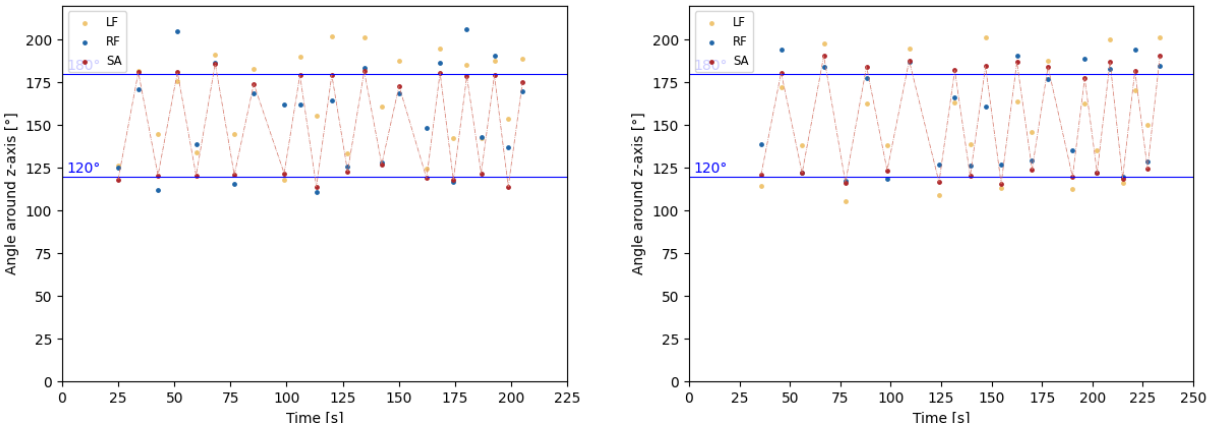

(a) Participant 1. **(b)** Participant 2.

Figure A4: Angle around the z-axis [°] versus time [s] of the prescribed angle of 120°. For a more elaborate explanation 10.

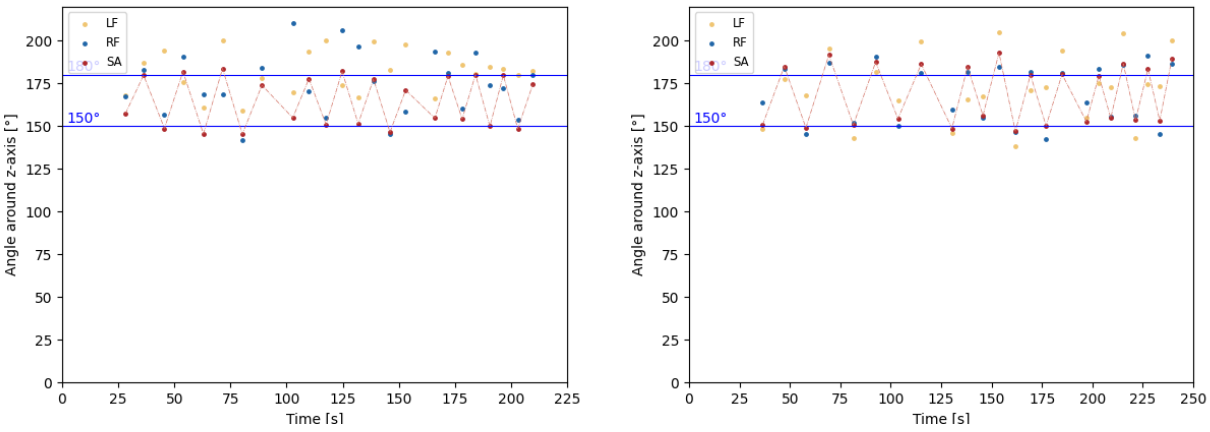

(a) Participant 1. **(b)** Participant 2.

Figure A5: Angle around the z-axis [°] versus time [s] of prescribed angle of 150°. For a more elaborate explanation 10.

The next two figures present the trend the data suggests as can be seen in figure A6 and A7 of Participants 1 and 2. In this figure the measured angle [°] versus the expected angle [°] of all angles is presented while separating the data of the slow, the preferred and the fast walking speeds. A linear polyfit trendline of those three subsets is also presented in these figures. It can be seen that all three trendlines are almost identical.

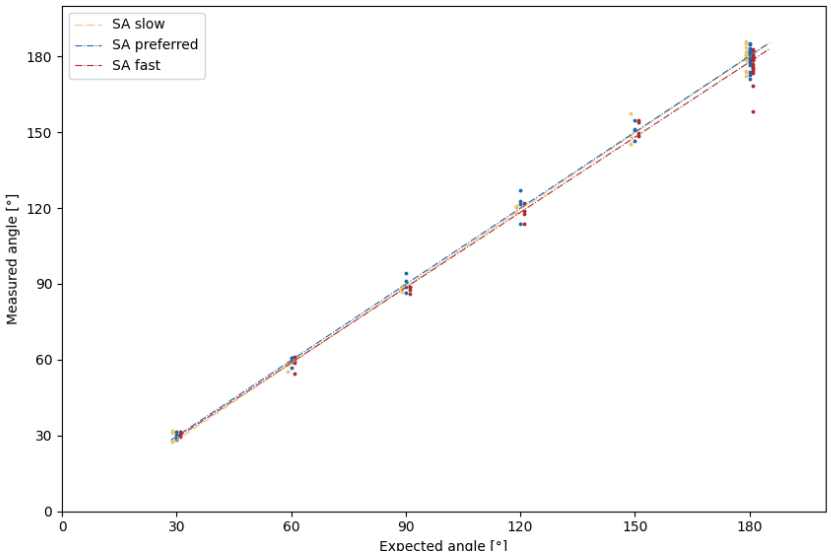

Figure A6: Measured angle [°] versus expected angle [°] of all prescribed angles of Participant 1. Where single data points are presented by dots and the trend is a linear polyfit trendline based on those data points. The slow speed of the SA data is denoted by yellow, the preferred speed of the SA data as blue and the fast speed of the SA data as red.

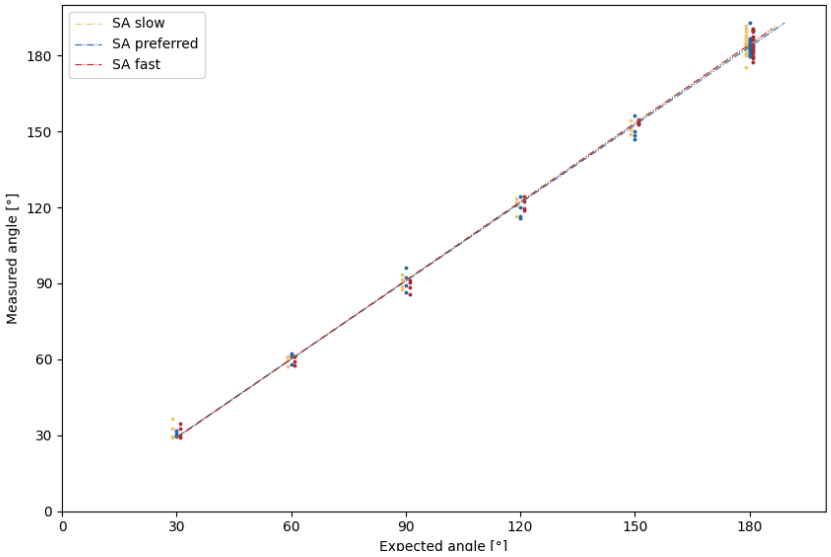

Figure A7: Measured angle [°] versus expected angle [°] of all prescribed angles of Participant 2. See figure A6 for a more detailed explanation.

The final figures, figure A8 and A9, present the absolute error of the data compared to its expected value. In these two figures the measured angle [°] versus the expected angle [°] is presented while separating the data of the slow, the preferred and the fast walking speeds of Participants 1 and 2. It can be seen that the LF and the RF have an enormous error compared to the SA.

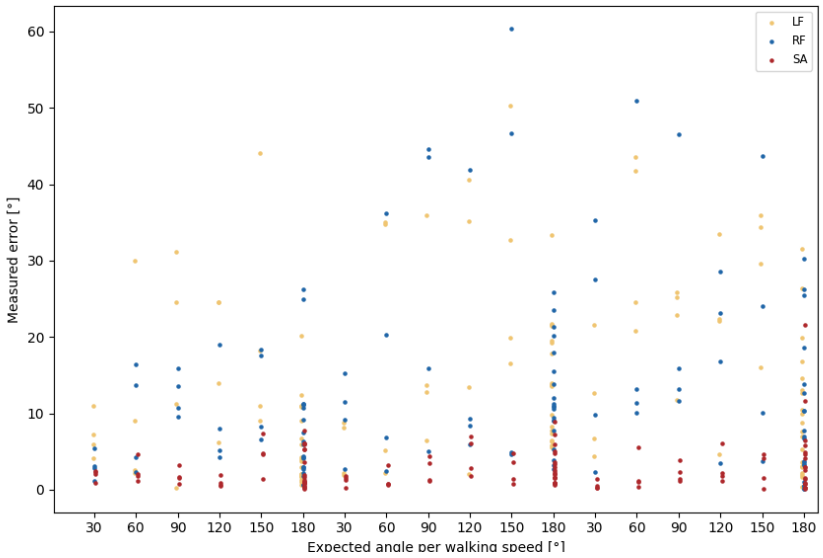

Figure A8: Measured error [°] versus expected angle [°] for all three walking speeds of Participant 3. The LF is represented by yellow, the RF by blue and the SA by red. Each walking speed is presented in its interval of 30°to 180°with on the left the slow speed, in the middle the preferred speed and on the right the fast speed of the LF, RF and SA.

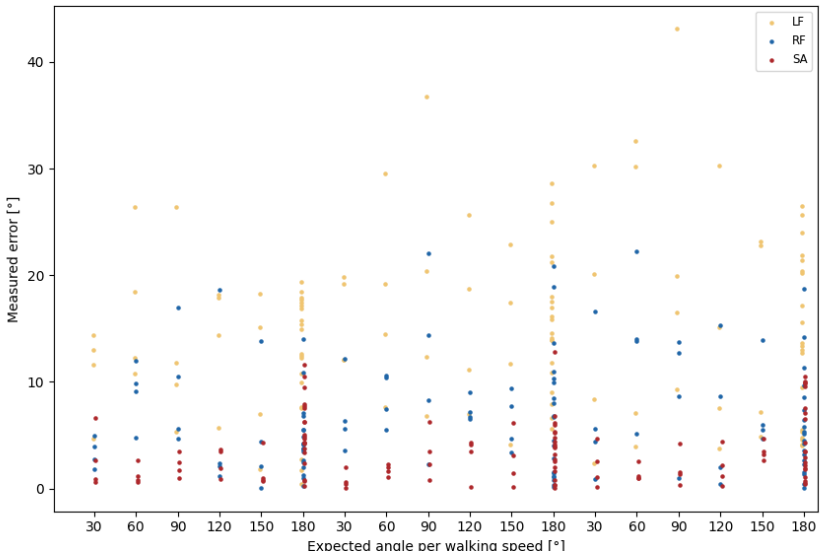

Figure A9: Measured error [°] versus expected angle [°] for all three walking speeds of Participant 4. The LF is represented by yellow, the RF by blue and the SA by red. Each walking speed is presented in its interval of 30°to 180°with on the left the slow speed, in the middle the preferred speed and on the right the fast speed of the LF, RF and SA.